University of Baghdad
College of Engineering
JE
JOURNAL OF ENGINEERING

Journal of Engineering
journal homepage: www.jcoeng.edu.iq
Volume 32 Number 4 April 2026

Nuclear Electromagnetic Moments of Odd-Mass Nuclei within Skyrme-Hartree-Fock-Bogoliubov and Shell-Model Frameworks

Murtadha H. Hasan*, Ali A. Alzubadi

Department of Physics, College of Science, University of Baghdad, Baghdad, Iraq

ABSTRACT

Accurate prediction of electromagnetic moments in odd-A nuclei near doubly magic cores is challenging due to their sensitivity to core polarization and single-particle structure. This study investigates the predictive performance of Skyrme-HFB (SLy4) against shell model (SM) calculations for quadrupole moment (Q_{20}) and magnetic dipole (M_{10}) in the selected nuclei (^{17}O, ^{17}F, ^{39}Ca, ^{39}K, ^{47}Ca, ^{49}Sc, ^{131}In, ^{133}Sb, ^{133}Sn, and ^{209}Bi) near doubly magic cores using the Hartree-Fock-Bogoliubov (HFB) method and the SM method. The SLy4 interaction was used in HFB calculations. On the other hand, SM calculations were performed in *sd, sd-pf*, *fp*, and *jj* shells using USDC, SDPF-U, GXPF1A, jj45pn, and sn100pn interactions. The calculated results of both methods were compared with experimental data from the IAEA/INDC nuclear datasets. For Q_{20} Skyrme-HFB predicted the correct sign with minor deviations in the value of light nuclei (e.g., ^{17}O, ^{17}F, ^{39}Ca, ^{47}Ca) by about −7% to +6%, but for heavier nuclei like ^{39}K and ^{49}Sc the deviation is much higher about (-88% and -85.7%), and for nuclei around ^{132}Sn and ^{208}Pb cores (^{131}In, ^{133}Sb, ^{133}Sn, ^{209}Bi) the deviation was also high, ranging from -81% to -96%. Meanwhile, the SM Q_{20} results showed a significant improvement, with a deviation of 1-16% for the whole set. For M_{10}, HFB calculations were close to experiment for light nuclei (^{17}O and ^{17}F) with deviation (0.99% and 1.53%), respectively, and reasonable for nuclei like (^{47}Ca ≈ 4.5% and ^{39}Ca ≈ 11.5%), but deviated strongly for ^{39}K by -73.87%. M_{10} for heavier nuclei was not evaluated within HFB in the present work. SM calculation reproduced M_{10} with absolute percent deviations of (0.03% − 29.23%) across the studied nuclei (median $|\Delta\%| \approx 8.09\%$), where the lowest $|\Delta\%|$ values were ^{17}F (0.03%), ^{209}Bi (0.29%), ^{39}K (0.38%), and ^{17}O (0.87%), while the highest $|\Delta\%|$ values were ^{39}Ca (29.23%), ^{133}Sn (25.53%), and ^{133}Sb (23.33%).

Keywords: Shell model, Hartree-Fock-Bogoliubov (HFB) method, Electromagnetic moments, Odd-mass nuclei, Nuclear deformation, Time-odd fields.

1. INTRODUCTION

Electric quadrupole (Q_{20}) and magnetic dipole (M_{10}) moments provide essential information about nuclei, such as nuclear shape and structure. The study of these moments is one of the

*Corresponding author
Peer review under the responsibility of University of Baghdad.
https://doi.org/10.31026/j.eng.2026.04.09

Article received: 27/12/2025
Article revised: 17/03/2026
Article accepted: 29/03/2026
Article published: 01/04/2026

most crucial fields in nuclear physics, especially for nuclei far from stability, where experimental studies are limited **(Harding et al., 2020; Koszorús et al., 2024; Stone, 2024)**. New measurement techniques for moment, such as collinear laser spectroscopy, have significantly improved accuracy. This allowed for a precise comparison of the mean-field (MF) and SM predictions across the nucleus set **(Harding et al., 2020; Koszorús et al., 2024)**.

The nuclei studied in this work are one particle or one hole away from the doubly magic cores, with both Z and N as magic numbers (8, 20, 28, 50, and 82). They are considered good probes for study, as they are close to spherical systems with one valence nucleon outside the closed shell, in which their Q_{20} values are sensitive to the detailed outer-particle configuration and core polarization. This is what makes good benchmarks for both SM calculations and the HFB approach **(Alzubadi and Allawi, 2021; Sassarini et al., 2022; Sassarini, 2023)**. Additionally, many of the chased nuclei have precise experimental Q_{20} and M_{10} values from high-resolution hyperfine-structure and laser-spectroscopy measurements, making them a clean test group for theoretical approaches **(Sassarini et al., 2022; Sassarini, 2023)**.

Calculating electromagnetic (EM) moments in odd-mass nuclei is way tougher than in even-mass systems. Due to the time-odd component activation and time-reversal symmetry breaking in the energy density functional (EDF), terms like these are not found in even-even configurations **(Spevak et al., 1997; Bonnard et al., 2023)**. In the Skyrme-HFB approach, it is possible to calculate them because time-even and time-odd fields are both present in the total energy equation **(Dobaczewski and Dudek, 1995)**. Thus, it is more sensitive for calculating odd-mass nuclei, particularly for the EM observables, especially M_{10}. Furthermore, the treatment of these nuclei necessitates the blocking of a quasiparticle. This blocking modifies the matrices to accurately represent the occupied configuration, thereby influencing the total energy and EM outcomes.

In the HFB framework, the blocking condition $\alpha_k^\dagger|\mathrm{HFB}\rangle = 0$ defines the occupation of a chosen quasiparticle state. This modification adds terms to the self-consistency loop and extends the calculations **(Bertsch et al., 2009)**. **(Sassarini et al., 2022)** showed that the mean field (MF) generally appears easier, especially when pairing interactions are weak, and that time-odd fields continue to be significant even in the vicinity of closed shells. Nuclear deformation and EM moments have been thoroughly investigated within both the SM and HFB frameworks. In the case of light nuclei, such as ^{7}Li, ^{19}F, and ^{27}Al, Shell Model calculations successfully reproduce the experimentally measured EM properties **(Harby and Alzubadi, 2022)**. For nuclei within the medium and heavy mass ranges, including the transitional isotopes in even-even nuclei, self-consistent HFB methods provide a dependable characterization of deformation. **(Alzubadi and Abdulhasan, 2015; Alzubadi et al., 2015; Alzubadi and Obaid, 2019)**. **(Dobaczewski et al., 1984; Dobaczewski and Dudek, 1995; Schunck et al., 2017)** highlighted the importance of time-odd MFs within the Skyrme-HFB framework, particularly concerning odd-mass nuclei.

The objective of this work is to calculate the Q_{20} and M_{10} moments of some odd nuclei near doubly magic cores (^{17}O, ^{17}F, ^{39}Ca, ^{39}K, ^{47}Ca, ^{49}Sc, ^{131}In, ^{133}Sb, ^{133}Sn, and ^{209}Bi) within the HFB framework of nuclear density functional theory (DFT), using the SLy4 interaction **(Dobaczewski et al., 2009; 2021; Schunck et al., 2017)**, and the SM calculations using related valence spaces (*sd, sd-pf, fp*, and *jj* shells) and modern effective interactions (USDC, SDPF-U, GXPF1A, jj45pn, sn100pn). Then the Q_{20} and M_{10} results were compared with the experimental values from the IAEA dataset referenced as **(Mertzimekis, 2016;**

Mertzimekis et al., 2016; Stone, 2024). Even- and odd-mass are both considered, with a special focus on how pairing in time-odd MFs influences nuclear deformation and EM properties.

2. THEORY AND METHODOLOGY

2.1 Hartree-Fock-Bogoliubov Formalism

The HFB method treats pairing correlations within nuclear DFT self-consistently, where the total energy is a functional of the one-body densities and the pairing tensor.

$$\alpha_k^\dagger \sum_l \left(U_{lk} c_l^\dagger + V_{lk} c_l\right) \tag{1}$$

where $c_l^\dagger, c_l$ are the operators are responsible for single-particle creation and annihilation, respectively, and U_{lk}, V_{lk} represent Bogoliubov amplitudes in the HFB equations. Blocking a quasiparticle state in odd-mass systems activates the time-odd fields of the Skyrme EDF and breaks the time-reversal symmetry **(Engel et al., 1975)**.

2.1.1 Currents and Local Densities

The EDF primarily relies on local densities and currents derived from one-body density matrices. For q nucleon (q=p, n for protons or neutrons), respectively:
The particle density

$$\rho_q(\mathbf{r}) = \sum_k V_k^2 \, |\phi_k(\mathbf{r})|^2 \tag{2}$$

kinetic density

$$\tau_q(\mathbf{r}) = \sum_k V_k^2 \, |\nabla\phi_k(\mathbf{r})|^2 \tag{3}$$

spin density and spin-current tensor

$$\mathbf{s}_q(\mathbf{r}) \;\; J_{q,\mu\nu}(\mathbf{r}) \tag{4}$$

where ρ_q, τ_q, s_q, and $J_{q,\mu\nu}$ are particle, kinetic, spin, and spin-current densities for nucleon q.

2.1.2 Energy Density Functional

The total HFB energy functional of the nuclear Hamiltonian is written as **(Beiner et al., 1975)**.

$$E = E_{\text{kin}} + E_{\text{Sk}} + E_{\text{Coul}} + E_{\text{pair}} \tag{5}$$

The equations for kinetic, Skyrme, Coulomb, and pairing energies are defined below from Eqs. (6) to (8):

$$E_{\text{kin}} = \frac{\hbar^2}{2m} \int d^3 r \tau_0(\boldsymbol{r}) - \frac{\hbar^2}{2mA} \int d^3 r \rho_0(\boldsymbol{r}) \tag{6}$$

$$E_{\text{Sk}} = \int d^3 r \sum_{t=0,1} \left(C_t^\rho \rho_t^2 + C_t^{\Delta\rho} \rho_t \Delta\rho_t + C_t^\tau \rho_t \tau_t + C_t^J J_t^2 + C_t^{\nabla J} \rho_t \nabla \cdot \boldsymbol{J}_t\right), \tag{7}$$

$$E_{\text{pair}} = -\sum_{q=n,p} G_q \sum_{k>0} u_{kq}\, v_{kq} \tag{8}$$

where τ_0 is the mathematical sum of τ_n and τ_p, A represents the mass number, ρ_0 is the sum of ρ_n and ρ_p, t = 0, 1 are the isoscalar and isovector, respectively, C_t is the constants of Skyrme coupling, u_{kq} and v_{kq} are Bogoliubov occupation amplitudes of state k for nucleon type q, and their product denotes the probability amplitude for scattering two nucleons into time-reversed states, and G_q is the pairing strength **(Da Costa et al., 2024; Shi et al., 2024)**.

$$E_{\text{Coul}} = \frac{1}{2}\int d^3\, r d^3 r' \frac{\rho_p(\boldsymbol{r})\rho_p(\boldsymbol{r}')}{|\boldsymbol{r}-\boldsymbol{r}'|} - \frac{3}{4}\left(\frac{3}{\pi}\right)^{1/3} \int d^3\, r \rho_p^{4/3}(\boldsymbol{r}) \tag{9}$$

In this equation, the first term is the direct Coulomb interaction, and the second is the exchange contribution in the Slater approximation.
The seniority-type pairing interaction, which comes from the older SM ideas, is presented in the constant-G form, as shown in Eq. (8), and the parameter G_q determines the pairing correlation strength among nucleons. Although schematic, it captures the essential physics of Cooper pairing near the Fermi surface and connects to the Bardeen–Cooper–Schrieffer (BCS) limit of HFB. In HFODD, the pairing interaction is computed through a mixed surface-volume density-dependent force,

$$V_{\text{pair}}^{(q)}(\boldsymbol{r}_1, \boldsymbol{r}_2) = V_0^{(q)} \left(1 - \frac{\rho(\frac{r_1+r_2}{2})}{\rho_0}\right) \delta(\boldsymbol{r}_1 - \boldsymbol{r}_2), \tag{10}$$

where $V_0^{(q)}$ represents the pairing strength for nucleon q (protons or neutrons), ρ and ρ_0 denote the local isoscalar and nuclear saturation densities, respectively, and $\delta(\boldsymbol{r}_1 - \boldsymbol{r}_2)$ is the Dirac delta function defining a zero-range pairing force. This mixed approach reduces pairing in the interior and strengthens it near the surface, thereby providing a realistic description of pairing gaps in medium- and heavy-mass nuclei.

2.1.3 Constrained HFB Equations

To obtain deformed solutions, the Routhian is minimized:

$$E' = E - \sum_{\lambda\mu} C_{\lambda\mu} (\langle \hat{Q}_{\lambda\mu} \rangle - Q^0_{\lambda\mu})^2 - \omega \langle \hat{J}_y \rangle - \sum_q \lambda_q \langle \hat{N}_q \rangle \tag{11}$$

Where $C_{\lambda\mu}$ represent the stiffness constants, $\hat{Q}_{\lambda\mu}$ and $Q^0_{\lambda\mu}$ are the multipole mass operators and target values, respectively, ω is the cranking frequency around *the y-axis*, $\langle \hat{J}_y \rangle$ is the angular momentum operator, and λ_q represents the Lagrange multipliers imposing the neutron and proton numbers $\hat{N}_q$. That means, E is the actual binding energy, while E' is the energy that is used in HFB self-consistent iteration. $C_{\lambda\mu}$ act as the spring constants, the targets $Q^0_{\lambda\mu}$ set the desired shape coordinates, the multipole operators $\hat{Q}_{\lambda\mu}$ Quantify the shape degrees of freedom. In the present work, no cranking calculations were performed; therefore, the rotational frequency was set to $\omega = 0$ for all nuclei.

2.2 Electromagnetic Operators

The EM observables can be written in terms of the spherical tensors. **(Titin-Schnaider and Quentin, 1974)**:

$$\hat{Q}_{2\mu} = e\sum_{i=1}^{Z} r_i^2\, Y_{2\mu}(\hat{r}_i), \quad \widehat{M}_{1\mu} = \sqrt{\frac{3}{4\pi}}\sum_{i=1}^{A}\left(g_l^{(i)}\hat{l}_{i,\mu} + g_s^{(i)}\hat{s}_{i,\mu}\right) \tag{12}$$

where $Y_{2\mu}$ is the spherical harmonics, r_i represents the position of (i) nucleon, $g_l^{(i)}$, $g_s^{(i)}$ represents the gyromagnetic orbital and spin factors, and $\hat{l}_{i,\mu}$, $\hat{s}_{i,\mu}$ are the angular momentum operators for orbital and spin, respectively. Then we can write the intrinsic quadrupole and M_{10} moments as follows:

$$Q_{20} = \langle\Phi|\hat{Q}_{20}|\Phi\rangle, \quad M_{10} = \langle\Phi|\widehat{M}_{10}|\Phi\rangle \tag{13}$$

with $|\Phi\rangle$ the HFB self-consistent state.
The quadrupole parameter for deformation analysis is

$$\beta_2 = \frac{4\pi}{3AR_0^2}Q_{20}, \quad R_0 = 1.A^{1/3}\text{fm}, \tag{14}$$

2.3 Shell-Model Framework

The many-body Schrödinger equation has an exact solution within the chosen valence space, for an effective Hamiltonian:

$$H_{SM} = \sum_i \epsilon_i\, a_i^\dagger a_i + \frac{1}{4}\sum_{ijkl} V_{ijkl} a_i^\dagger a_j^\dagger a_l a_k, \tag{15}$$

where it contains two terms:

a) Single-particle term

$$\sum_i \epsilon_i\, a_i^\dagger a_i \tag{16}$$

where: i is the index label of single particle orbital quantum numbers $i \equiv (n_i, l_i, j_i, m_i, t_i)$, and these quantum numbers are the radial, orbital, total angular momentum, angular momentum projection, and isospin, respectively. ϵ_i is the single-particle energy of the orbital i.

b) Two-body interaction term

$$\frac{1}{4}\sum_{ijkl} V_{ijkl} a_i^\dagger a_j^\dagger a_l a_k \tag{17}$$

where V_{ijkl} is the two-body matrix elements of the effective interaction $V_{ijkl} = \langle ij|V_{ijkl}|kl\rangle$. The matrix term shows the residual interaction between pairs of nucleons in the valence space. The diagonalization of H_{SM} give us the eigenstates that are used to compute Q20 and M_{10} **(Brussaard and Glaudemans, 1977; Alzubadi and Harby, 2023)**.

2.3.1 Valence Spaces and Inert Cores

For each nucleus in this study, a standard valence space was chosen based on the nucleus mass region and its close doubly magic core. These vacancies are:

sd-shell → (^{17}O, ^{17}F) build on ^{16}O core, sd-pf shells → (^{39}Ca, ^{39}K) build on ^{40}Ca core, fp-shell → (^{47}Ca, ^{49}Sc) out of ^{48}Ca core, jj45pn-type → (^{131}In, ^{133}Sb, ^{133}Sn) based on Sn core, and finally, jj56pn-type → ^{209}Bi build on ^{208}Pb core. These SM are consistent in this mass region **(Brussaard and Glaudemans, 1977; Sultan and Alzubadi, 2025)**.

`

2.3.2 Effective Interactions

Modern, effective interactions were used that were specifically developed for these mass regions. For sd-shell MS, the USDC Hamiltonian was chosen, which is one of the new USD-type interactions that deal with the isospin-breaking terms, and provides an improved description of sd-shell spectroscopy. **(Magilligan and Brown, 2020)**. The SD-PF was calculated with the SDPF-U interaction, which is good for large-scale calculations in this region. And it has been successfully applied to nuclei with Z = 8-20 and N = 20-40 **(Nowacki and Poves, 2009)**. For the fp-shell GXPF1A interaction was used, and this interaction is an improved version of the GXPF1 Hamiltonian that reproduces a wide range of spectroscopic data across the pf-shell **(Honma et al., 2005)**. And for jj45pn MS, we used two interactions, the jj45pna interaction, which is an effective Hamiltonian interaction based on the G-matrix, works above a ^{78}Ni core. **(Maurya et al., 2013)**, and the sn100pn interaction, which is widely employed for nuclei close to ^{100}Sn, is based on a CD-Bonn G-matrix **(Majeed, 2006)**. Finally, for jj56pn, the realistic interaction used, which is extensively used to decipher spectroscopy in heavy nuclei, with $A \approx 210$ **(Warburton and Brown, 1991; Gaudefroy, 2010)**.

2.3.2 Electromagnetic Operators

Q_{20} and M_{10} are obtained in the SM through the one-body EM operators, which can be converted to a many-body matrix element using the one-body transition density matrix (OBDM). The OBDM is defined as

$$OBDM(f,i,k_a k_b,\lambda) = \frac{\left\langle f \left\| \left[a^{\dagger}_{k_a} \otimes \tilde{a}_{k_b}\right]^{\lambda} \right\| i \right\rangle}{\sqrt{2\lambda+1}} \tag{18}$$

where f, i are the final and initial many-body nuclear states, each of which represents all the quantum numbers, k_a, k_b are the single particle orbitals, λ is the multipolarity (e.g., $\lambda = 2$ for E2, $\lambda = 1$ for M1), $a^{\dagger}_{k_a}$ is the creation operator for a nucleon in an orbital k_a, $\tilde{a}^{\dagger}_{k_a}$ is the time-reversed, angular-momentum annihilation operator for orbital k_b.
Then we use

$$\left\langle f \left\| X^{(\lambda)} \right\| i \right\rangle = \sum_{k_a k_b} OBDM(f,i;k_a k_b;\lambda) \left\langle k_a \left\| X^{(\lambda)} \right\| k_b \right\rangle \tag{19}$$

where $X^{(\lambda)}$ is a general matrix element operator (can be O(E2), O(M1), $T^{(\lambda)}$, etc.).
So, for any state with angular momentum J we can write Q_{20} *and* M_{10} respectively as **(Alzubadi and Harby, 2023)**:

$$Q(J) = \sqrt{\frac{16\pi}{5}} \begin{pmatrix} J & 2 & J \\ -J & 0 & J \end{pmatrix} \sum_{t_z=p,n} \left\langle J \left\| \hat{O}(E2)^{t_z} \right\| J \right\rangle, \tag{20}$$

where $\hat{O}(E2)^{t_z}$ is the one-body E2 operator acting on protons and neutrons.

$$\mu(J) = \sqrt{\frac{4\pi}{3}} \begin{pmatrix} J & 1 & J \\ -J & 0 & J \end{pmatrix} \sum_{t_z=p,n} \langle J \| \hat{O}(M1)^{t_z} \| J \rangle \ \mu_N, \quad (21)$$

where μ_N is the nuclear magneton and $\hat{O}(M1)^{t_z}$ is the one-body M1 operator, and $\begin{pmatrix} J & \lambda & J \\ -J & 0 & J \end{pmatrix}$ is the 3j symbol coming from the Wigner-Eckart factor with $(M_f = M_i = J, q = 0)$. Also, we should notice that the residual core-polarization effects that are not included in the model spaces are absorbed into phenomenological effective charges and effective spin g-factors **(Brussaard and Glaudemans, 1977)**.

2.4 Computational Tools

Hartree–Fock–Bogoliubov calculations were performed with HFODD (v3.06h) using the Skyrme SLy4 energy density functional. The single-particle wave functions were expanded in a deformed harmonic-oscillator basis, including up to $N_{max} = 12$ major shells for light nuclei and $N_{max} = 14$ shells for nuclei near ^{132}Sn and ^{208}Pb. The oscillator frequency followed the standard prescription $\hbar\omega = 41A^{-1/3}$MeV. Self-consistency was achieved with an energy convergence criterion better than 10^{-6}MeV. Pairing correlations were treated with a mixed surface-volume density-dependent zero-range interaction and a quasiparticle cutoff of 60 MeV. For odd-mass nuclei, self-consistent quasiparticle blocking was applied; several configurations consistent with the experimental spin-parity were tested, and the lowest-energy solution was retained. Time-reversal symmetry was broken in odd-A systems, while axial and reflection symmetries were conserved. Shell-model calculations were carried out using NuShellX@MSU in the appropriate valence spaces outside the ^{16}O, ^{40}Ca, ^{132}Sn, and ^{208}Pb cores. The interactions employed were USDC, SDPF-U, GXPF1A, jj45pna, sn100pn, and the standard jj56pn interaction for the heavy region. Full diagonalizations were performed within the chosen model spaces. Effective charges of $e_p = 1.3e$, $e_n = 0.5e$(sd–pf regions) and $e_p = 1.5e$, $e_n = 0.8e$(jj region) were adopted for quadrupole operators. Magnetic dipole moments were calculated using free orbital g-factors and quenched spin g-factors $g_s^{\text{eff}} = 0.7\, g_s^{\text{free}}$.

3. RESULTS AND DISCUSSION

In this section, we discuss the theoretical results from both HFB with the Skyme nuclear DFT and the SM calculation, along with the available experimental data for the selected odd nuclei near doubly magic cores. The analysis focuses on the comparison between HFB and SM results. We arrange the results in four tables. **Tables 1 and 2** are the Q_{20} and both HFB and SM, respectively. And the same for M_{10} in **Tables 3 and 4**. Finally, we simulated the shape of each nucleus to illustrate the deformation.

3.1 HFB Quadrupole Moments

As mentioned, the Skyrme-HFB calculated Q_{20} and the experimental values, with their deviations, are summarized in **Table 1**. The HFB quantities are the intrinsic axial Q_{20} moments, which are extracted from the self-consistent density as mentioned in the methodology section, and the experimental values are spectroscopic (lab-frame) Q_{20}. Therefore, the mapping from intrinsic to spectroscopic moments is approximate and may not be guaranteed in near-spherical (magic/near-magic) systems.

Table 1. HFB Q_{20} (in barns) for odd nuclei near doubly magic cores, with the experimental values. The J^{π} values and the deviation between theoretical and experimental are included.

Isotopes	J^{π}	$Q_{20}^{\mathrm{HFB}}\ (b)$	$Q_{20}^{Exp}\ (b)$	$\Delta\% = (HFB - Exp)/Exp$
O-17	5/2+	-0.0238	-0.0256 ±0.0002*	-7.0%
F-17	5/2+	0.0758	0.076 ±0.004*	-0.3%
Ca-39	3/2+	0.0362	0.038 ±0.003*	-4.7%
K-39	3/2+	0.0724	0.603 ±0.006*	-88.0%
Ca-47	7/2-	0.0893	0.084 ±0.006*	6.3%
Sc-49	7/2-	-0.0228	-0.159 ± 0.008**	-85.7%
In-131	9/2+	0.0130	0.31 ± 0.01**	-95.8%
Sb-133	7/2+	-0.0321	-0.304 ± 0.007**	-89.4%
Sn-133	7/2-	-0.0260	-0.145 ± 0.010**	-82.1%
Bi-209	9/2-	-0.0976	-0.516 ±0.015*	-81.1%

* The experimental data from ref. **(Mertzimekis, 2016; Mertzimekis et al., 2016)**
** The experimental data from ref. **(Sassarini et al., 2022)**

From the deviations and **Fig. 1**, it is evident that the light nuclei ^{17}O, ^{17}F, and ^{39}Ca, as well as the ^{47}Ca, are reproduced with the sign and magnitude correctly by the HFB approach, by relative deviations of the order of a few percent. $\Delta Q/Q_{exp}$ values are relatively good, about −7.0% for ^{17}O, −0.3% for ^{17}F, −4.7% for ^{39}Ca, and +6.3% for ^{47}Ca. In these cases, the odd nucleon moves in a single orbital outside a doubly magic core, and the mean-field configuration captures the core's small polarization responsible for the observed precise Q_{20}.

For ^{39}K and ^{49}Sc, a different behavior was found. The HFB calculations reproduce the experimental sign of Q_{20}, but the magnitudes are strongly inaccurate. For ^{39}K, the deviations are about -88%. Similarly, for ^{49}Sc, about -85.7%. These deviations can be amplified near closed shells due to the highly sensitive EM moments to the detailed polarization and blocking configuration. Additionally, sensitivity to the blocking strategies can vary across different blocked quasiparticles, and therefore Q_{20} can change strongly; this is well known in odd-mass EDF calculations **(Sassarini, 2023; Li et al., 2024)**. EM moments depend on polarization (including time-odd fields) more than bulk observables; SLy4 is not optimized for moments, and time-odd pairing details can shift results, particularly in heavier and weakly deformed nuclei **(Bonnard et al., 2023; Sassarini, 2023)**.

In the ^{132}Sn and ^{208}Pb regions. For the odd-mass nuclei ^{131}In, ^{133}Sb, ^{133}Sn, and ^{209}Bi, the HFB calculations reproduce the experimental sign of the Q_{20}, but the magnitude is nearly one order smaller than the empirical ones. The relative deviations reach -95.8% for ^{131}In, -89.4% for ^{133}Sb, -82.1% for ^{133}Sn, and -81.1% for ^{209}Bi. And this deviation appears clearly in **Fig. 1**. Measured experimental moment for odd-A neighbors near doubly magic cores can be sizable even when the nucleus is essentially spherical, and the single-reference HFB density can still show too spherical, yielding to a small deformation (small intrinsic Q_{20}) **(Dobaczewski et al., 2025)**. Also, static moments in odd-A nuclei are strongly affected by the time odd MF. Standard Skyrme parametrizations are primarily fitted to bulk properties, whereas time-odd couplings are less constrained, which leads to systematic drift in moments **(Lyutorovich, 2024)**. While mean-field results often perform well for bulk observables in medium-heavy nuclei, EM moments for odd nuclei near magic cores are a challenging benchmark due to their enhanced dependence on time-odd polarization and the absence of symmetry restoration in this study **(Bonnard et al., 2023)**.

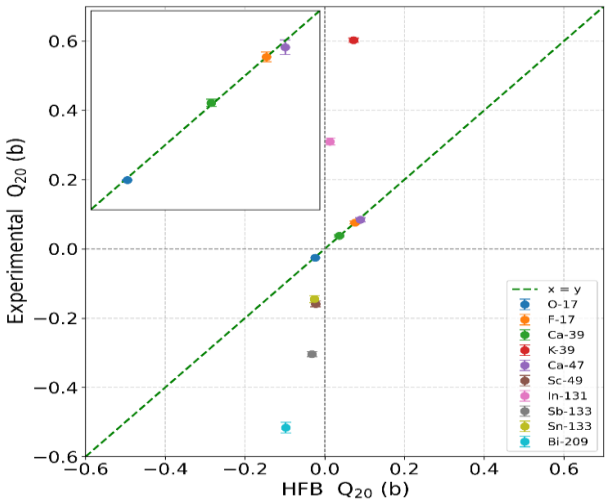

Figure 1. Comparison of HFB calculated quadrupole moments Q_{20} with experimental values for the chosen nuclei set. The diagonal line indicates perfect agreement.

3.2 Shell-Model Quadrupole Moments

The SM quadrupole moments collected in **Table 2** show a remarkable improvement over the HFB results for most of the studied nuclei. This appears clearly as shown in **Fig. 2**, where most of the data lies on the perfect agreement, the diagonal line. In the sd-shell region, the USDC interaction combined with effective charges ep=1.3e and en=0.5e reproduces very well the experimental moments of ^{17}O and ^{17}F.

Table 2. Quadrupole moments Q_{20}(in barns) for odd nuclei near doubly magic cores by SM calculations and the experimental data. Spin-parity assignments and relative MS, Effective Interaction, and Effective Charge are all listed.

Isotopes	J^{π}	Q_{20}^{SM} (b)	Q_{20}^{Exp} (b)	Model Space	Effective Interaction	Effective Charge	Δ%
O-17	5/2+	-0.027	-0.0256 ±0.0002*	*sd*	USDC	e_p=1.3, e_n=0.5	0.055
F-17	5/2+	0.082	0.076 ±0.004*	*sd*	USDC	e_p=1.3, e_n=0.5	0.079
Ca-39	3/2+	0.0331	0.038 ±0.003*	*sdpf*	SDPF-U	e_p=1.3, e_n=0.5	-0.129
K-39	3/2+	0.070	0.603 ±0.006*	*sdpf*	SDPF-U	e_p=1.3, e_n=0.5	-0.884
Ca-47	7/2-	0.090	0.084 ±0.006*	*fp*	GXPF1A	e_p=1.3, e_n=0.5	0.071
Sc-49	7/2-	-0.150	-0.159 ± 0.008**	*fp*	GXPF1A	e_p=1.3, e_n=0.5	-0.057
In-131	9/2+	0.360	0.31 ± 0.01**	*jj45pn*	jj45pna	e_p=1.5, e_n=0.8	0.161
Sb-133	7/2+	-0.270	-0.304 ± 0.007**	*jj45pn*	jj45pna	e_p=1.5, e_n=0.8	-0.112
Sn-133	7/2-	-0.000	-0.145 ± 0.010**	*jj45pn*	sn100pn	e_p=1.5, e_n=0.8	-1
Bi-209	9/2-	-0.520	-0.516 ±0.015*	*jj56pn*	realistic	e_p=1.5, e_n=0.8	0.008

* The experimental data from ref. **(Mertzimekis, 2016; Mertzimekis et al., 2016)**
** The experimental data from ref. **(Sassarini et al., 2022)**

For these nuclei, the calculated values are close to the experimental Q_{20} values. with relative deviations of the order of a few percent. A similarly good agreement is obtained for the fp-shell nucleus ^{47}Ca, where the GXPF1A interaction with the same set of effective charges yields $Q_{20}^{SM} = 0.090\ b$, to be compared with the experimental value $Q_{20}^{exp} = 0.084\ b$. For ^{49}Sc, the SM value $Q_{20}^{exp} = -0.150$ b also follows the experimental result -0.159 b closely.

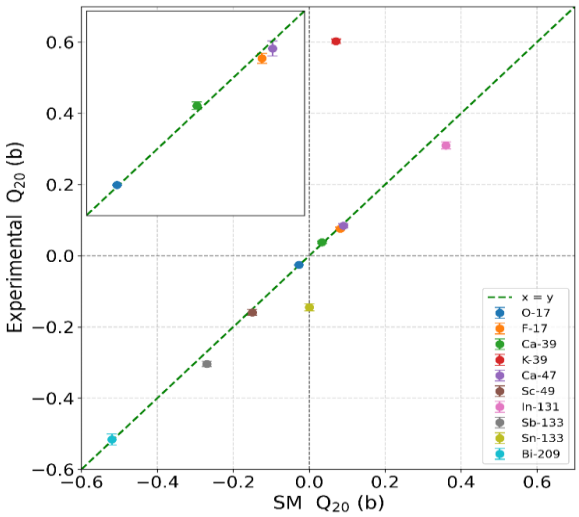

Figure 2. Comparison between SM Q_{20} and the experimental values for the chosen nuclear set. The diagonal line indicates perfect agreement.

3.3 Comparison between HFB and Shell-Model Q_{20}

A direct comparison of HFB and SM calculated values appears clearly in **Fig. 3**, where the diagonal line shows the perfect agreement between the two approaches. The light nuclei are shown as agreed in the zoomed window of the figure. Also, by reading **Tables 1 and 2** it appears that the SM systematically outperforms the Skyrme-HFB approach in reproducing the experimental Q_{20}.

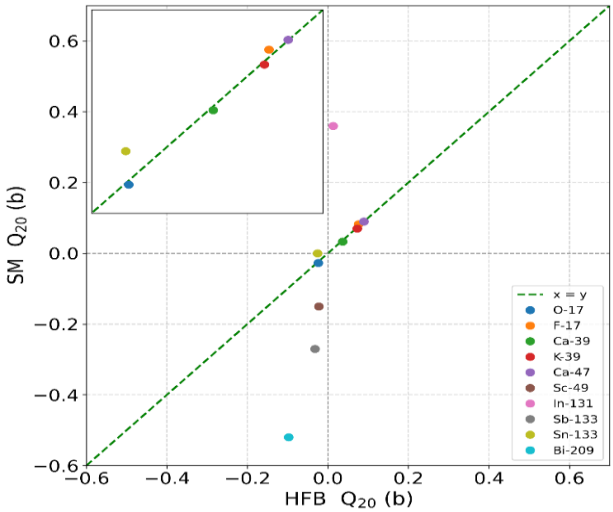

Figure 3. Comparison of HFB calculated quadrupole moments $Q_{20}$with SM values for chosen nuclei set. The diagonal line indicates perfect agreement.

In the light nucleus regions (^{17}O, ^{17}F, ^{39}Ca, ^{47}Ca, ^{49}Sc), the HFB calculations provide a reasonable description. They predict the correct sign of Q_{20} and achieve relative deviations at the level of a few percent in most cases. However, the SM results for the same nuclei are closer to the experimental data, within the experimental uncertainties, showing how the configuration-interaction framework can capture detailed configuration mixing and core polarization effects when phenomenological effective charges and effective spin g-factors are employed.

3.4 HFB Magnetic Dipole Moments

The M_{10} obtained from the Skyrme-HFB calculations and the relative deviations from the experiment are summarized in **Table 3.** The nuclei ^{17}O and ^{17}F, the HFB approach performs remarkably well, and the calculated values $\mu^{HFB} = -1.9122\ \mu_N$ and $\mu^{HFB} = 4.7934\ \mu_N$ differ from the experimental moments $\mu^{exp} = -1.893543\mu_N$ and $\mu^{exp} = 4.7213\mu_N$ by only about 0.99% and 1.53%, respectively. For ^{47}Ca, the HFB result $\mu^{HFB} = -1.4702\,\mu_N$ and the experimental value $\mu^{exp} = -1.4064\,\mu_N$, with a deviation of about 4.54%. But the results are somehow less satisfactory in ^{39}Ca, where the calculated magnetic moment $\mu^{HFB} = 1.1389\,\mu_N$ mismatch the empirical value $\mu^{exp} = 1.0214\,\mu_N$ by approximately 11.5%, which is a relatively large deviation. Nevertheless, the sign and overall magnitude are correctly reproduced, showing that the mean-field description still captures the main features of the spin-orbit structure and core polarization in this nucleus. For the heavier nuclei ^{49}Sc, ^{131}In, ^{133}Sb, ^{133}Sn, and ^{209}Bi, only experimental (or reference) values of the M_{10} moments are listed in **Table 3**, while the corresponding HFB moments were not evaluated in the present work. In these systems, the interplay between complex configuration mixing in the valence space and the poorly constrained time-odd terms makes fully self-consistent calculations particularly sensitive. Therefore, the comparison between theory and experiment for M_{10} moments in the heavy region will be restricted in this study to the SM result.

Table 3. HFB Magnetic dipole moments M_{10}^{HFB} (in μ_N) for the chosen nuclear. All Experimental data are from the IAEA dataset **(Mertzimekis, 2016; Mertzimekis et al., 2016)**.

Isotopes	J^{π}	$M_{10}^{\mathrm{HFB}}\ (\mu_N)$	$M_{10}^{Exp}\ (\mu_N)$	$\Delta\% = (HFB - Exp)/Exp$
O-17	5/2+	-1.9122	-1.893543 ± 1e-05	0.99%
F-17	5/2+	4.7934	4.7213 ± 0.0003	1.53%
Ca-39	3/2+	1.1389	1.0214 ± 0.00016	11.50%
K-39	3/2+	0.1023	0.39147 ± 8e-06	-73.87%
Ca-47	7/2-	-1.4702	-1.4064 ± 0.0011	4.54%
Sc-49	7/2-	-	5.61 ± 0.03	-
In-131	9/2+	-	6.312 ± 0.014	-
Sb-133	7/2+	-	3 ± 0.04	-
Sn-133	7/2-	-	-1.41 ± 0.001	-
Bi-209	9/2-	-	4.092 ± 0.002	-

3.5 Shell-Model Magnetic Dipole Moments

The SM magnetic dipole moments listed in **Table 4** show better agreement with experiment than in the HFB results, especially in the sd and fp regions. For the sd-shell nuclei ^{17}O and ^{17}F, calculated with the USDC interaction and standard effective charges $e_p = 1.3e$, $e_n = 0.5e$, the SM values $\mu^{SM} = -1.91\,\mu_N$ and $\mu^{SM} = 4.72\,\mu_N$ are extremely close to the experimental moments -1.893543 μN and 4.7213 μN, respectively. The deviations are well below the percent level and comparable to those obtained in the HFB approach, confirming that both frameworks can reproduce these benchmark moments when the underlying single-particle structure is dominated by a single valence orbital. A similarly excellent agreement is found for ^{39}K, where the SM prediction $\mu^{SM} = 0.39\,\mu_N$ almost exactly reproduces the experimental value $\mu^{exp} = 0.39147\ \mu_N$. While in the heavy jj-shell region, the SM again reproduces the sign and magnitude precisely, although with somewhat larger inconsistency.

Table 4. Shell-Model Magnetic dipole moments M_{10}^{SM} (in μ_N) for the chosen nuclear set. All Experimental data are from the IAEA dataset **(Mertzimekis, 2016; Mertzimekis et al., 2016)**.

Isotopes	J^{π}	M_{10}^{SM} (μ_N)	M_{10}^{Exp} (μ_N)	Model Space	Effective Interaction	Effective Charge	Δ%
O-17	5/2+	-1.91	-1.893543 ± 1e-05	*sd*	USDC	e_p=1.3, e_n=0.5	0.009
F-17	5/2+	4.72	4.7213 ± 0.0003	*sd*	USDC	e_p=1.3, e_n=0.5	0.000
Ca-39	3/2+	1.32	1.0214 ± 0.00016	*sdpf*	SDPF-U	e_p=1.3, e_n=0.5	0.292
K-39	3/2+	0.39	0.39147 ± 8e-06	*sdpf*	SDPF-U	e_p=1.3, e_n=0.5	-0.004
Ca-47	7/2-	-1.52	-1.4064 ± 0.0011	*fp*	GXPF1A	e_p=1.3, e_n=0.5	0.081
Sc-49	7/2-	4.56	5.61 ± 0.03	*fp*	GXPF1A	e_p=1.3, e_n=0.5	-0.187
In-131	9/2+	5.80	6.312 ± 0.014	*jj45pn*	jj45pna	e_p=1.5, e_n=0.8	-0.081
Sb-133	7/2-	3.70	3 ± 0.04	*jj45pn*	jj45pna	e_p=1.5, e_n=0.8	0.233
Sn-133	7/2-	-1.05	-1.41 ± 0.001	*jj45pn*	sn100pn	e_p=1.5, e_n=0.8	-0.255
Bi-209	9/2-	4.08	4.092 ± 0.002	jj56pn	realistic	e_p=1.5, e_n=0.8	-0.003

For ^{131}In and ^{133}Sb, calculated with the jj45pna interaction, the SM moments $\mu^{SM} = 5.80\,\mu_N$ and $3.70\,\mu_N$ are smaller and larger, respectively, than the experiment values 6.312 μN and 3.0 μN, corresponding to deviations of order 10-20%. For ^{133}Sn, the predicted moment $\mu^{SM} = -1.05\,\mu_N$ underestimates the empirical value -1.41 μN, while for ^{209}Bi, the SM calculation yields $\mu^{SM} = 4.08\,\mu_N$, in almost perfect agreement with $\mu^{exp} = 4.092\,\mu_N$. These results demonstrate that, even in the challenging jj-shell region, configuration-interaction calculations with realistic interactions and modestly quenched g-factors provide a largely satisfactory description of ground-state M_{10} moments in odd nuclei near doubly magic cores, consistent with earlier SM analyses of EM moments in similar systems **(Lechner et al., 2023; Shukla et al., 2024)**.

3.6 Nuclear Deformation and Shape Simulation

To visualize the evolution of nuclear shape along the chosen nuclei set, nuclear deformation was plotted in the fore figures, **Figs. 4 to 7,** HFB calculated data being listed in **Figs. 4 and 5** for light and heavy nuclei, respectively, and the same flow in **Figs. 6 and 7** for the SM approach. The deformation parameter β_2 was calculated for all Q_{20} values of each nucleus, due to the dimensionless characterization of β_2. Using the standard relation below **(Ring and Schuck, 1983)**:

$$\beta_2 = \frac{4\pi}{3ZR^2} Q_{20} \tag{22}$$

Where: R Is the nuclear radius calculated from the mass number $R = r_0(A)^{\frac{1}{3}}$ choosing $r_0 = 1.2\ fm$, Z is the representation of the atomic number, and A is the mass number of each nucleus.

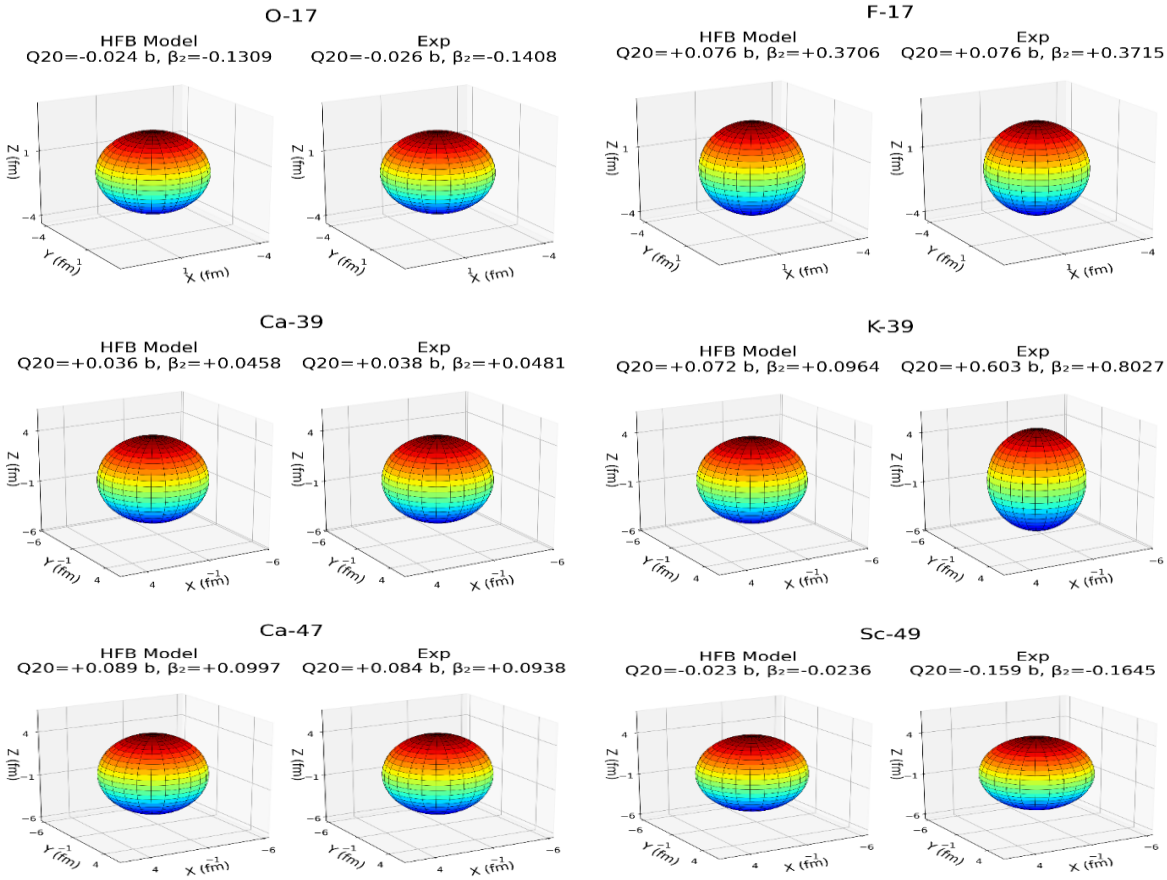

Figure 4. Axial deformation simulation for HFB calculated values (left side) and experimental (right side), for light nuclei of the chosen nuclear set. Shapes are derived from deformation parameters β_2.

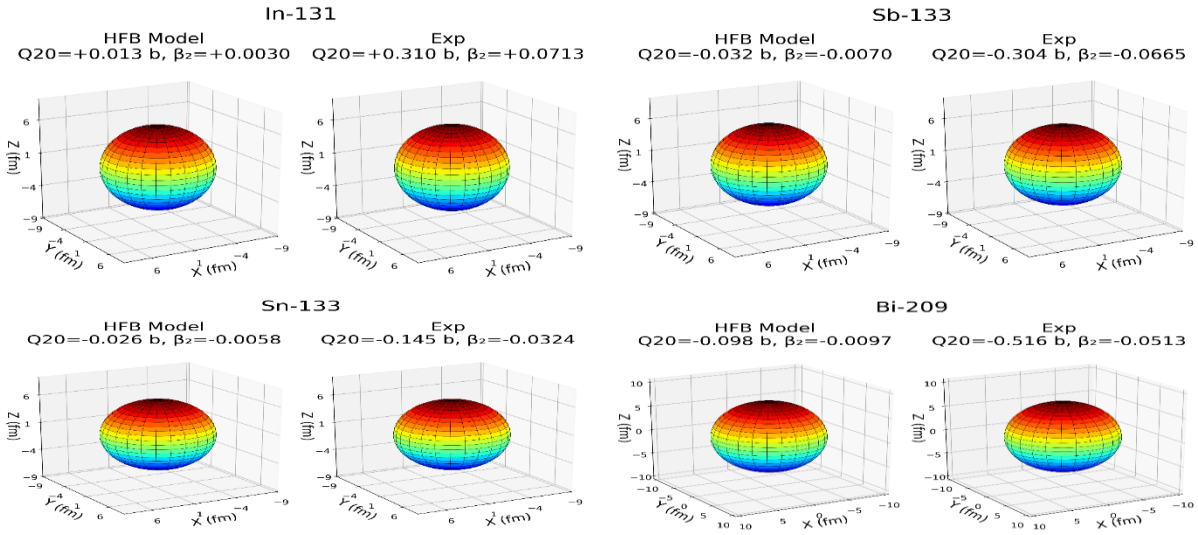

Figure 5. Axial deformation simulation for HFB calculated values (left side) and experimental (right side), for heavy nuclei of the chosen nuclear set. Shapes are derived from deformation parameters β_2.

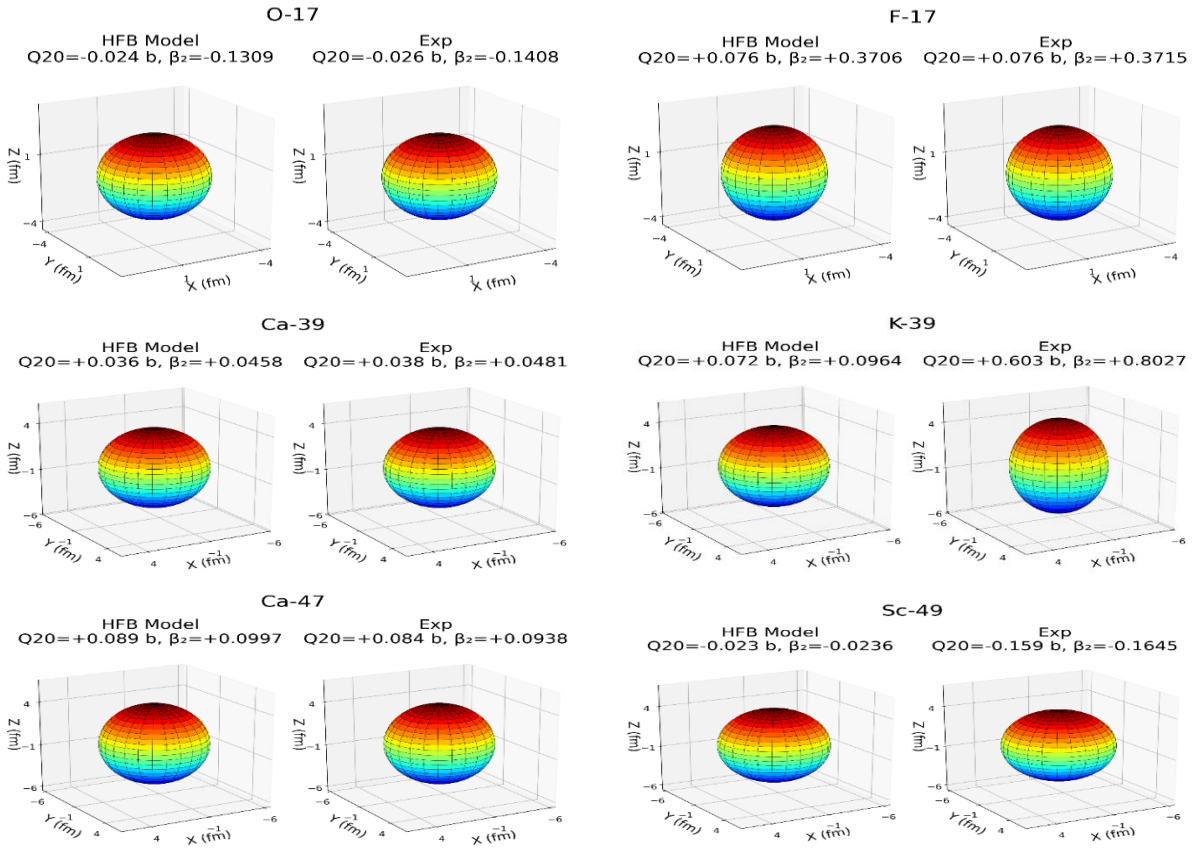

Figure 6. Axial deformation simulation for SM calculated values (left) and experimental (right), for light nuclei of the chosen nuclear set. Shapes are derived from deformation parameters β_2.

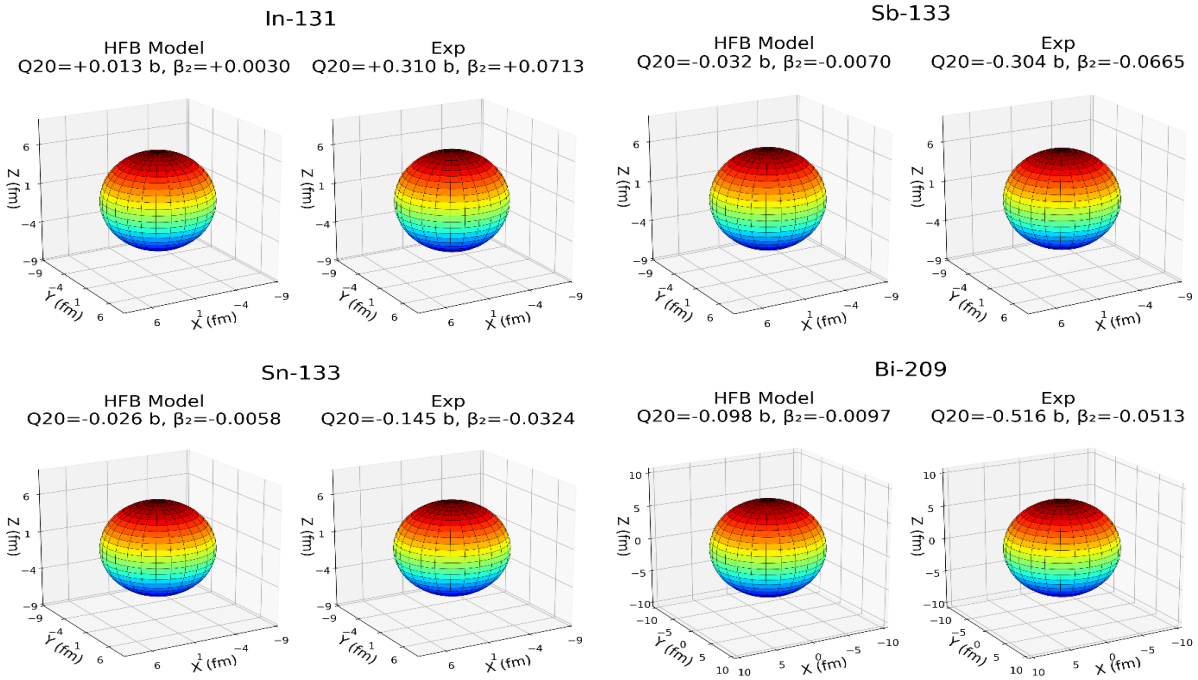

Figure 7. Axial deformation simulation for SM calculated values (left) and experimental (right), for heavy nuclei of the chosen nuclear set. Shapes are derived from deformation parameters β_2.

With this conversion, the dependence on mass number is removed for Q_{20} values. What allows for a straightforward comparison across the set. The deformation parameter β_2 was used to shape the ellipsoid according to the formula:

$$a = R(1 - 0.15\beta_2), \qquad c = R(1 + 0.3\beta_2) \tag{23}$$

where a represents the radius across the equator on the x and y plane, c represents the polar radius on the z-direction, and R is the radius of the nucleus, the 0.15 and 0.3 factors in Eq. (23), are chosen to ensure the nuclear volume conservation and surface linearization **(Bohr and Mottelson, 1975; Harding et al., 2020)**. The β_2 magnitude and its sign indicate the degree of prolateness or oblateness of the nuclear shape. A Python script is used to plot the 3D ellipsoid that shows both theoretical and experimental deformation and their differences. These visualizations help clarify the models and compare results, bridging theory and geometric shape.

4. CONCLUSIONS

This work provides a benchmark of Skyrme-HFB (SLy4) versus shell-model calculations for Q_{20} and M_{10} in the odd-A nucleus, one-particle and one-hole neighbors of doubly magic cores, which are particularly challenging due to their sensitivity to core polarization and single-particle structure, and identifies the mass regions in which each approach is reliable. The electric quadrupole Q_{20} and magnetic dipole M_{10} Moments of odd-A nuclei, a large set (^{17}O, ^{17}F, ^{39}Ca, ^{39}K, ^{47}Ca, ^{49}Sc, ^{131}In, ^{133}Sb, ^{133}Sn, and ^{209}Bi) near doubly magic cores were investigated, using two complementary approaches: the Skyrme-HFB and shell-model calculations. Both were compared with the latest experimental values from the IAEA/INDC dataset. For Q_{20}, HFB results showed good agreement in the light-nucleus region (e.g., ^{17}O, ^{17}F, ^{39}Ca, ^{47}Ca) with a few percent deviation. However, for ^{39}K and ^{49}Sc, and the nuclei near ^{132}Sn and ^{208}Pb cores, the results were underestimated by about 80% to 96%. This behavior is most evident when the valence nucleon occupies high-j orbitals, where the quadrupole moments are strongly influenced by the particle-hole excitations and the core-polarization rather than the static deformation. These heavy cores are very rigid and nearly spherical under static deformation, yielding only weak intrinsic quadrupole polarization and significantly reduced Q values, by the blocked HFB solution. On the other hand, the SM explicitly incorporates configuration mixing and valence-core coupling. provides a more accurate description of Q_{20} across the set, with deviations of approximately 1%-16%, consistent with experimental data, supporting the importance of the configuration mixing picture. For M_{10}, HFB showed good agreement for ^{17}O and ^{17}F, and reasonable agreement for ^{47}Ca. Meanwhile, it shows a significant deviation for ^{39}K. Notice that the magnetic moment in the heavy region was not calculated in this study. On the SM side, M_{10} is reproduced accurately with $|\Delta\%| \approx 0.03\%$ *to* 29.23% with a median of (8.09). Overall, the results indicate that SLy4-HFB captures the correct trend and the light-region moments but shows large underestimation for selected $A \approx 40$ cases and near the ^{132}Sn and ^{208}Pb cores, whereas the shell model provides consistently quantitative agreements.

NOMENCLATURE

Symbol	Description	Symbol	Description
β_2	Quadrupole deformation parameter, dimensionless	μ_N	Nuclear magneton
C	Polar radius of nucleus, fm	Q_{20}	Electric quadrupole moment, b
C_t	Skyrme coupling constants	r	Radial coordinate, fm
E	Total HFB energy, MeV	R	Nuclear radius, fm
$J_{\{q,\mu\nu\}}$	Spin–current tensor	s_q	Spin density, fm^{-3}
M_{10}	Magnetic dipole moment, μ_N	τ_q	Kinetic density, fm^{-5}
ρ_q	Particle density for nucleon q, fm^{-3}	U_{lk}, V_{lk}	Bogoliubov amplitudes
λ_q	Particle-number Lagrange multiplier	$Y_{2\mu}$	Spherical harmonic

Credit of Authors Contribution

Murtadha H. Hasan: Writing – original draft, Validation, Software, Methodology. Ali A. Alzubadi: Reviewing & editing.

Declaration of Competing Interest

The authors declare that they have no known competing financial interests or personal relationships that could have appeared to influence the work reported in this paper.

REFERENCES

Alzubadi, A.A. and Abdulhasan, A.A., 2015. Nuclear deformation study using the framework of self-consistent Hartree-Fock-Bogoliubov. *Karbala International Journal of Modern Science*, 1(2), pp. 110–121. https://doi.org/10.1016/J.KIJOMS.2015.09.002

Alzubadi, A.A. and Allawi, R.A., 2021. Investigation of the magicity in some even–even Ca isotopes by using shell model and Hartree–Fock–Bogoliubov method. *Indian Journal of Physics 2021 96:4*, 96(4), pp. 1205–1216. https://doi.org/10.1007/S12648-021-02052-X

Alzubadi, A.A. and Harby, G.W., 2023. Calculation of the electromagnetic moments and electroexcitation form factors for some boron isotopes using shell model with Skyrme interaction. *Revista Mexicana de Física*, 69(1). https://doi.org/10.31349/REVMEXFIS.69.011202

Alzubadi, A.A., Latooffi, N.F., and Radhi, R.A., 2015. Shell model and Hartree-Fock calculations for some exotic nuclei. *International Journal of Modern Physics E*, 24(12). https://doi.org/10.1142/S0218301315500998

Alzubadi, A.A. and Obaid, R.S., 2019. Study of the nuclear deformation of some even–even isotopes using the Hartree–Fock–Bogoliubov method (effect of the collective motion). *Indian Journal of Physics*, 93(1), pp. 75–92. https://doi.org/10.1007/s12648-018-1269-2

Beiner, M., Flocard, H., Van Giai, N. and Quentin, P., 1975. Nuclear ground-state properties and self-consistent calculations with the Skyrme interaction. (I). Spherical description. *Nuclear Physics, Section A*, 238(1), pp. 29–69. https://doi.org/10.1016/0375-9474(75)90338-3

Bertsch, G., Dobaczewski, J., Nazarewicz, W. and Pei, J., 2009. Hartree-Fock-Bogoliubov theory of polarized Fermi systems. *Physical Review A*, 79(4), P. 043602. https://doi.org/10.1103/PhysRevA.79.043602

Bohr, A. and Mottelson, B.R., 1975. *Nuclear structure. Vol. 2, Nuclear deformations*. W. A. Benjamin, Inc.

https://openlibrary.org/works/OL1274866W/Nuclear_structure?edition=key%3A%2Fbooks%2FOL5631869M

Bonnard, J., Dobaczewski, J., Danneaux, G., and Kortelainen, M., 2023. Nuclear DFT electromagnetic moments in heavy deformed open-shell odd nuclei. *Physics Letters B*, 843, P. 138014. https://doi.org/10.1016/J.PHYSLETB.2023.138014

Brussaard, P.J. and Glaudemans, P.W.M., 1977. Shell-model applications in nuclear spectroscopy. *North Holland*. https://cir.nii.ac.jp/crid/1971430859852643599

Da Costa, P., Bennaceur, K., Meyer, J., Ryssens, W. and Bender, M., 2024. Impact of choices for center-of-mass correction energy on the surface energy of Skyrme energy density functionals. *Physical Review C*, 109(3). https://doi.org/10.1103/PhysRevC.109.034316

Dobaczewski, J., Backes, B.C., de Groote, R.P., Restrepo-Giraldo, A., Sun, X. and Wibowo, H., 2025. Electromagnetic and Exotic Moments in Nuclear DFT. http://arxiv.org/abs/2511.04632

Dobaczewski, J., Baczyk, P., Becker, P., Bender, M., Bennaceur, K., Bonnard, J., Gao, Y., Idini, A., Konieczka, M., Kortelainen, M., Próchniak, L., Romero, A.M., Satula, W., Shi, Y., Werner, T.R. and Yu, L.F., 2021. Solution of universal nonrelativistic nuclear DFT equations in the Cartesian deformed harmonic-oscillator basis. (IX) HFODD (v3.06h): A new version of the program. *Journal of Physics G: Nuclear and Particle Physics*, 48(10). https://doi.org/10.1088/1361-6471/ac0a82

Dobaczewski, J. and Dudek, J., 1995. Time-odd components in the mean field of rotating superdeformed nuclei. *Physical Review C*, 52(4), pp. 1827–1839. https://doi.org/10.1103/PhysRevC.52.1827

Dobaczewski, J., Flocard, H. and Treiner, J., 1984. Hartree-Fock-Bogolyubov description of nuclei near the neutron-drip line. *Nuclear Physics, Section A*, 422(1), pp. 103–139. https://doi.org/10.1016/0375-9474(84)90433-0

Dobaczewski, J., Satula, W., Carlsson, B.G., Engel, J., Olbratowski, P., Powalowski, P., Sadziak, M., Sarich, J., Schunck, N., Staszczak, A., Stoitsov, M., Zalewski, M. and Zdunczuk, H., 2009. Solution of the Skyrme-Hartree-Fock-Bogolyubov equations in the Cartesian deformed harmonic-oscillator basis. (VI) HFODD (v2.38j): a new version of the program. *Computer Physics Communications*, 180(11), pp. 2361–2391. https://doi.org/10.1016/j.cpc.2009.08.009

Engel, Y.M., Brink, D.M., Goeke, K., Krieger, S.J. and Vautherin, D., 1975. Time-dependent Hartree-Fock theory with Skyrme's interaction. *Nuclear Physics, Section A*, 249(2), pp. 215–238. https://doi.org/10.1016/0375-9474(75)90184-0

Gaudefroy, L., 2010. Shell model study of $N \simeq 28$ neutron-rich nuclei. *Physical Review C*, 81(6), P. 064329. https://doi.org/10.1103/PhysRevC.81.064329

Harby, G.W. and Alzubadi, Ali, A., 2022. Calculation of the Magnetic Dipole and Electric Quadrupole Moments of some Sodium Isotopes using Shell Model with Skyrme Interaction. *Iraqi Journal of Physics*, 20(3), pp. 40–49. https://doi.org/10.30723/IJP.V20I3.1004

Harding, R.D., Pallada, S., Croese, J., Antušek, A., Baranowski, M., Bissell, M.L., et al., 2020. Magnetic Moments of Short-Lived Nuclei with Part-per-Million Accuracy: Toward Novel Applications of ß -Detected NMR in Physics, Chemistry, and Biology. *Physical Review X*, 10(4), P. 041061. https://doi.org/10.1103/PhysRevX.10.041061

Honma, M., Otsuka, T., Brown, B.A., and Mizusaki, T., 2005. Shell-model description of neutron-rich pf-shell nuclei with a new effective interaction GXPF 1. *The European Physical Journal A - Hadrons and Nuclei 2005 25:1*, 25(1), pp. 499–502. https://doi.org/10.1140/EPJAD/I2005-06-032-2

Koszorús, Á., de Groote, R.P., Cheal, B., Campbell, P. and Moore, I.D., 2024. Nuclear structure studies by collinear laser spectroscopy. *European Physical Journal A*, 60(1), pp. 1–17. https://doi.org/10.1140/epja/s10050-024-01230-9

Lechner, S., Miyagi, T., Xu, Z.Y., Bissell, M.L., Blaum, K., Cheal, B., et al., 2023. Electromagnetic moments of the antimony isotopes 112–133Sb. *Physics Letters B*, 847, P. 138278. https://doi.org/10.1016/J.PHYSLETB.2023.138278

Li, T., Schunck, N. and Grosskopf, M., 2024. Multipole responses in fissioning nuclei and their uncertainties. *Physical Review C*, 110(3), P. 034317. https://doi.org/10.1103/PhysRevC.110.034317

Lyutorovich, N., 2024. Description of the odd 249-253No nuclei using Skyrme functionals with modified spin-spin interaction. *International Journal of Modern Physics E*, 33(7). https://doi.org/10.1142/S0218301324500277

Magilligan, A. and Brown, B.A., 2020. New isospin-breaking "USD" Hamiltonians for the sd shell. *Physical Review C*, 101(6), P. 064312. https://doi.org/10.1103/PhysRevC.101.064312

Majeed, F.A., 2006. Shell model study of even-even 132-134Te neutron-rich nuclei. 37. https://doi.org/10.48550/arXiv.nucl-th/0601084

Maurya, K., Srivastava, P.C. and Mehrotra, I., 2013. Shell Model Description of N = 51 Isotones. *IOSR Journal of Applied Physics (IOSR-JAP*, 3(4), pp. 52–59. https://doi.org/10.9790/4861-0345259

Mertzimekis, T.J., 2016. *Development of a dedicated online database for nuclear moments data*. *IAEA INDC Reports*. Vienna, Austria. https://doi.org/10.61092/IAEA.VSF9-639M

Mertzimekis, T.J., Stamou, K. and Psaltis, A., 2016. An online database of nuclear electromagnetic moments. *Nuclear Instruments and Methods in Physics Research, Section A: Accelerators, Spectrometers, Detectors and Associated Equipment*, 807, pp. 56–60. https://doi.org/10.1016/j.nima.2015.10.096

Nowacki, F. and Poves, A., 2009. New effective interaction for 0^{-}hω shell-model calculations in the sd-pf valence space. *Physical Review C*, 79(1), P. 014310. https://doi.org/10.1103/PhysRevC.79.014310

Ring, P. and Schuck, P., 1983. *The Nuclear Many-Body Problem*. *Physics Today*, AIP Publishing. https://doi.org/10.1063/1.2915762

Sassarini, P.L., 2023. *Nuclear Moments in Density Functional Theory: An analysis of magnetic dipole and electric quadrupole moments within nuclear DFT of one-particle and one-hole neighbours of doubly magic nuclei*. [MPhil thesis] University of York. https://etheses.whiterose.ac.uk/id/eprint/34700/7/Sassarini_206045222_CorrectedThesisClean.pdf

Sassarini, P.L., Dobaczewski, J., Bonnard, J., and Ruiz, R.F.G., 2022. Nuclear DFT analysis of electromagnetic moments in odd near doubly magic nuclei. *Journal of Physics G: Nuclear and Particle Physics*, 49(11), P. 11LT01. https://doi.org/10.1088/1361-6471/AC900A

Schunck, N., Dobaczewski, J., Satuła, W., Bączyk, P., Dudek, J., Gao, Y., Konieczka, M., Sato, K., Shi, Y., Wang, X.B. and Werner, T.R., 2017. Solution of the Skyrme-Hartree--Fock--Bogolyubov equations in the Cartesian deformed harmonic-oscillator basis. (VIII) hfodd (v2.73y): A new version of the

program. *Computer Physics Communications*, 216, pp. 145–174. https://doi.org/10.1016/j.cpc.2017.03.007

Shi, Y., Stevenson, P.D. and Hinohara, N., 2024. A program for 3D nuclear static and time-dependent density-functional theory with full Skyrme energy density functional: HIT3D. http://arxiv.org/abs/2403.12539

Shukla, S., Srivastava, P.C. and Patel, D., 2024. Systematic shell-model study of structure and isomeric states in 204–213Bi isotopes. *Journal of Physics G: Nuclear and Particle Physics*, 51(7), P. 075103. https://doi.org/10.1088/1361-6471/AD4D07

Spevak, V., Auerbach, N. and Flambaum, V. V., 1997. Enhanced T-odd, *P*-odd electromagnetic moments in reflection asymmetric nuclei. *Physical Review C*, 56(3), p.1357. https://doi.org/10.1103/PhysRevC.56.1357

Stone, N.J., 2024. Nuclear moments: recent developments. *Interactions*, 245(1), pp. 1–6. https://doi.org/10.1007/S10751-024-01896-Z

Sultan, L.F. and Alzubadi, A.A., 2025. Study of Nuclear Deformations for Some Nuclei located Near the Nuclear Island of Inversion Region. *Ibn AL-Haitham Journal for Pure and Applied Sciences*, 38(4), pp. 190–198. https://doi.org/10.30526/38.4.4146

Titin-Schnaider, C. and Quentin, P., 1974. Coulomb exchange contribution in nuclear Hartree-Fock calculations. *Physics Letters B*, 49(5), pp. 397–400. https://doi.org/10.1016/0370-2693(74)90617-0

Warburton, E.K. and Brown, B.A., 1991. Appraisal of the Kuo-Herling shell-model interaction and application to A=210–212 nuclei. *Physical Review C*, 43(2), P. 602. https://doi.org/10.1103/PhysRevC.43.602

العزوم الكهرومغناطيسية للنوى الفردية الكتلة ضمن إطاري سكريم-هارتري-فوك-بوغوليوبوف ونموذج القشرة

مرتضى حسين حسن*، علي عبد اللطيف الزبيدي

قسم الفيزياء، كلية العلوم، جامعة بغداد، بغداد، العراق

الخلاصة

إن التنبؤ الدقيق بالعزوم الكهرومغناطيسية في النوى الفردية الكتلة القريبة من القلوب مزدوجة السحر يُعد تحدياً نظراً لحساسيتها العالية لاستقطاب القلب النووي وبنية الجسيم المفرد. تهدف هذه الدراسة إلى تقييم القدرة التنبؤية لطريقة سكريم–هارتري–فوك–بوغوليوبوف (Skyrme-HFB) باستخدام التآثر SLy4 ومقارنتها بحسابات نموذج القشرة (SM) لعزم رباعي القطب الكهربائي (Q20) والعزم المغناطيسي ثنائي القطب (M10) في مجموعة مختارة من النوى وهي: ^{17}O,^{17}F,^{39}Ca، ^{39}K، ^{47}Ca، ^{49}Sc، ^{131}In,^{133}Sn, ^{133}Sb, ^{209}Bi القريبة من القلوب مزدوجة السحر، وذلك باستخدام طريقة هارتري–فوك–بوغوليوبوف (HFB) وطريقة نموذج القشرة. استُخدم التآثر SLy4 في حسابات HFB، بينما أُجريت حسابات نموذج القشرة ضمن الأغلفة النووية sd وsd-pf وfp وjj باستخدام التأثرات الفعّالة USDC وSDPF-U وGXPF1A وjj45pn وsn100pn. وقد جرى مقارنة النتائج المحسوبة في كلا الطريقتين مع البيانات التجريبية المستمدة من قواعد بيانات العزوم النووية التابعة للوكالة الدولية للطاقة الذرية IAEA/INDC. بالنسبة إلى العزم رباعي القطب الكهربائي Q_{20}، تنبأت حسابات Skyrme-HFB بالإشارة الصحيحة مع انحرافات طفيفة في قيم النوى الخفيفة مثل (^{17}O, ^{17}F, ^{39}Ca, ^{47}Ca) تراوحت بين −7% و +6%. إلا أن الانحراف كان أكبر بكثير في نوى أثقل مثل ^{39}K و^{49}Sc حيث بلغ نحو −88% و−85.7% ، كما كان كبيراً أيضاً في النوى القريبة من القلوب ^{132}Sn و^{208}Pb مثل(^{131}In, ^{133}Sb, ^{133}Sn, ^{209}Bi) ، حيث تراوح بين −81% و−96%. في المقابل، أظهرت نتائج نموذج القشرة تحسناً واضحاً في قيمQ_{20} ، إذ تراوحت نسبة الانحراف ضمن 1%–16% عبر مجموعة النوى المدروسة. أما بالنسبة إلى العزم المغناطيسي ثنائي القطبM_{10} ، فقد كانت نتائج HFB قريبة من القيم التجريبية في النوى الخفيفة (17F, 17O). بانحراف قدره 0.99% و1.53% على التوالي، وكانت معقولة أيضاً في نوى مثل ^{47}Ca حوالي 4.5% و^{39}Ca بحوالي 11.5%، لكنها انحرفت بشدة في النواة ^{39}K بنسبة −73.87%. ولم يتم في هذه الدراسة حساب قيم M_{10} للنوى الثقيلة باستخدام طريقةHFB. من جهة أخرى، أعادت حسابات نموذج القشرة إنتاج قيم M_{10} بانحرافات مئوية مطلقة تراوحت بين 0.03% و 29.23%عبر مجموعة النوى المدروسة بوسيط ($|\Delta\%| \approx 8.09$). وقد سُجلت أصغر قيم $|\Delta\%|$ في النوى ^{17}F (0.03%) و^{209}Bi (0.29%) و^{39}K (0.38%) و^{17}O(0.87%)، في حين ظهرت أكبر القيم في النوى ^{39}Ca (29.23%) و^{133}Sn (25.53%)و^{133}Sb(23.33%).

الكلمات المفتاحية: نموذج القشرة، طريقة هارتري-فوك-بوغوليوبوف، العزوم الكهرومغناطيسية، النوى الفردية الكتلة، التشوه النووي، الحقول الفردية الزمنية.